Journal of
Materials in Life Sciences

Vol. 4 No. 1 (2025)

Full Paper

Eco-Friendly Fabrication of *Persicaria odorata*-Silver Nanoparticles-Kaolinite Composite and Its Efficacy as Antibacterial Agent

Imran Qashfi Ismail[a], Nik Ahmad Nizam Nik Malek[ab]*, Muhammad Hariz Asraf[c],Juan Matmin[bd]

[a]Department of Biosciences, Faculty of Science, Universiti Teknologi Malaysia, 81310 UTM Johor Bahru, Johor, Malaysia.
[b]Centre for Sustainable Nanomaterials, Universiti Teknologi Malaysia, 81310 UTM Johor Bahru, Johor, Malaysia.
[c]Asraf Life Resources, Cubex03, Innovation & Commercialisation Centre, Industry Centre, UTM Technovation Park, 81300 Skudai, Johor, Malaysia
[d]Department of Chemistry, Faculty of Science, Universiti Teknologi Malaysia, 81310 UTM Johor Bahru, Johor, Malaysia.

Article history
Received
30 April 2025
Revised
10 May 2025
Accepted
26 May 2025
Published online
31 May 2025

*Corresponding author
niknizam@utm.my

Abstract

This study presents the green synthesis of silver nanoparticle-incorporated kaolinite (K-AgNP-Kaol) using *Persicaria odorata* leaf extract as a natural reducing and capping agent. The biosynthesis was optimized by adjusting extract volume and reaction temperature, with optimal AgNP formation achieved at 0.6 mL of extract and 80°C, as indicated by a surface plasmon resonance (SPR) peak at 431 nm. Structural and morphological characterizations were conducted using Fourier Transform Infrared Spectroscopy (FTIR), Field Emission Scanning Electron Microscopy (FESEM), Transmission Electron Microscopy (TEM), and Energy Dispersive X-ray Spectroscopy (EDX), confirming the successful incorporation of AgNPs into the kaolinite matrix without compromising its structural integrity. Antibacterial activity was evaluated against *Escherichia coli* (Gram-negative), *Staphylococcus aureus*, and *Cutibacterium acnes* (both Gram-positive) through disc diffusion, minimum inhibitory concentration (MIC), and minimum bactericidal concentration (MBC) assays. The K-AgNP-Kaol composite exhibited inhibitory effects against all tested strains, with enhanced efficacy in deionized water compared to saline, likely due to reduced silver ions in the solution because of silver chloride (AgCl) formation in the saline solution. These findings highlight K-AgNP-Kaol as a promising, eco-friendly antibacterial material suitable for broad-spectrum applications.

Keywords *Silver nanoparticles, Kaolinite composite, Green synthesis, Antibacterial activity, Persicaria odorata extract*

1.0 INTRODUCTION

Nanobiotechnology has garnered significant attention due to its wide-ranging applications in areas such as cancer drug delivery, molecular imaging, and antimicrobial therapy. At the core of this field are nanoparticles, which are materials with dimensions typically between 1 and 100 nm, can be classified into organic, inorganic, and ceramic categories (Ijaz et al.,

2020). Among them, silver nanoparticles (AgNPs), a type of inorganic metal nanoparticle, have been extensively explored for their distinctive physicochemical and biological properties. Notably, AgNPs exhibit strong surface plasmon resonance (SPR) phenomena, which give rise to unique optical and electronic characteristics (Asraf et al., 2024). The exceptional properties of nanoparticles arise from their high surface area-to-volume ratio, nanoscale size, surface charge, porosity, and morphology. These features, along with their crystalline or amorphous structures and varied shapes (e.g., spherical, rod-like, hexagonal), influence their reactivity and functional performance. Additionally, environmental factors such as light, humidity, and temperature can further modulate nanoparticle behaviour (Ijaz et al., 2020).

Nanoparticle synthesis techniques are generally categorized into top-down and bottom-up approaches. Top-down methods, including mechanical milling and lithography, often rely on physical processes, while bottom-up techniques encompass chemical vapour deposition, pyrolysis, and biological synthesis. However, many physical and chemical methods involve toxic reagents or harsh conditions, limiting their use in biomedical applications (Li et al., 2011). In response, green synthesis, particularly via biological routes, has emerged as an environmentally friendly and safer alternative, utilizing natural resources like plant extracts to mediate nanoparticle formation (Asraf et al., 2024).

Among various metallic nanoparticles, green-synthesized AgNPs have shown potent antimicrobial activity and are of growing interest in biomedical and environmental applications (Asraf et al., 2022; Dakal et al., 2016; Din et al., 2022). The use of plant-based reducing and stabilizing agents offers a sustainable pathway for AgNP production, with minimal ecological impact. *Persicaria odorata*, a Southeast Asian herb, has recently been reported as an effective biogenic agent, enhancing AgNP synthesis while imparting desirable antibacterial, cytocompatibility, and wound healing properties (Lubis et al., 2022). Despite its promise, the potential of *P. odorata* as a dual-function reducing and capping agent remains underexplored.

Notably, AgNPs are prone to aggregation, which can reduce their surface area and compromise their antimicrobial efficacy. To overcome this limitation, a stable carrier system such as kaolinite is required to support uniform dispersion and enhance the stability of AgNPs. Kaolinite, a naturally abundant clay mineral composed of tetrahedral silica and octahedral alumina sheets ($Al_2Si_2O_5(OH)_4$), is known for its high cation exchange capacity and biocompatibility (Chi, 1999). Its layered structure enables effective incorporation of bioactive agents. Previous applications have demonstrated its efficacy in loading antibacterial compounds, such as chlorhexidine (Isah et al., 2020), and pesticides, like amitrole (Tan et al., 2015). Building on this foundation, the paper presents a study on kaolinite-based nanocomposites embedded with biosynthesized AgNPs using *P. odorata* extract and evaluates its antibacterial efficacy against Gram-positive and Gram-negative bacterial strains.

2.0 EXPERIMENTAL

2.1 Materials

Kaolinite KM40 was obtained from Kaolin (M) Sdn. Bhd., Perak, Malaysia. Silver nitrate ($AgNO_3$) was purchased from Sigma-Aldrich. Fresh *P. odorata* leaves were sourced from a local market. All microbiological media and broths, including Reinforced Clostridium Medium (RCM), bacterial agar, and Luria-Bertani (LB) broth, were supplied by Oxoid.

2.2 Preparation of Materials

The aqueous extract of *P. odorata* was prepared by first separating the fresh leaves from stems, followed by drying in an oven at 60°C for 48 hours. The dried leaves were ground into fine powder using a laboratory grinder. A total of 2 g of the powdered leaves was added to 100 mL of deionized water and heated with continuous stirring at 100°C for 30 minutes. The mixture was filtered using Whatman No. 1 filter paper, and the extract was stored at 4 °C until further use.

The synthesis of silver nanoparticle-loaded kaolinite (K-AgNP-Kaol) was carried out via an in-situ method. Specifically, 2 g of kaolinite was added to 50 mL of 1 mM $AgNO_3$ solution and stirred continuously for 24 hours. Following this, the optimized volume of *P. odorata* extract was added to the suspension and stirred for another 24 hours (Asraf et al., 2024). The resulting mixture was filtered using Whatman No. 1 filter paper and subsequently dried in an oven at 40°C overnight. The dried composite was stored in dark conditions prior to characterization. Control samples were also prepared with slight modifications to the procedure. For the Kesum-Kaol sample, kaolinite was mixed only with *P. odorata* extract, excluding $AgNO_3$. Conversely, the Ag-Kaol sample was prepared by combining kaolinite with $AgNO_3$ solution only, omitting the plant extract. A biosynthesized AgNP sample was also prepared without kaolinite. The resulting materials were designated as kaolinite (Kaol), silver-kaolinite (Ag-Kaol), silver nanoparticle-loaded kaolinite (K-AgNP-Kaol), and biosynthesized silver nanoparticles (AgNP).

2.3 Characterization of Materials

Characterization of the synthesized materials was performed using various analytical techniques. Attenuated Total Reflectance Fourier-Transform Infrared Spectroscopy (ATR-FTIR) was conducted using a Nicolet iS50 instrument over the

range of 400–4000 cm^{-1} to identify functional groups. Field Emission Scanning Electron Microscopy (FESEM, MAIA3 LMH) and Transmission Electron Microscopy (TEM, ThermoFisher Scientific Talos L120C G2, 120 kV) were employed to observe surface morphology and particle distribution. Prior to imaging, samples were coated with platinum using a sputter coater. Additionally, Energy Dispersive X-ray Spectroscopy (EDX) was used to determine the elemental composition and confirm the presence of silver in the nanocomposites.

2.4 Antimicrobial Assay

2.4.1 Disc Diffusion Technique

The antibacterial activity of the synthesized samples was initially assessed using the disc diffusion technique (DDT) against *Escherichia coli*, *Staphylococcus aureus*, and *Cutibacterium acnes*. Since the samples were in powdered form, they were compressed into pellets using a mechanical press. For the assay, three to four colonies of *E. coli* and *S. aureus* were inoculated into the nutrient broth and their turbidity was adjusted to 0.5 McFarland standard. The suspensions were then streaked evenly on Mueller-Hinton Agar (MHA) plates. The prepared pellets were placed on the agar surface and incubated overnight at 37°C in an inverted position. A similar procedure was used for *C. acnes*, which was incubated in an anaerobic environment using a sealed tank system. Inhibition zones around the pellets were observed and measured to determine antibacterial effectiveness.

2.4.2 Minimum Inhibition Concentration

The Minimum Inhibitory Concentration (MIC) assay was conducted to determine the lowest concentration of the sample required to inhibit bacterial growth. Bacterial suspensions were prepared and centrifuged at 4000 rpm for 15 minutes, followed by washing with distilled water. The bacterial pellets were then resuspended in either deionized water or 0.9% saline. Each sample namely kaolinite, K-AgNP-Kaol, AgNP, Kesum-Kaol, and Ag-Kaol was tested at concentrations of 0.01, 0.03, 0.06, 0.09, and 0.12 g. To each 10 mL bacterial suspension, the respective sample was added and incubated at 37°C for 30 minutes with agitation at 100 rpm. The mixtures were then allowed to stand for 5 minutes. Subsequently, 10 µl from each tube was plated onto nutrient agar (NA) and incubated overnight at 37°C. Bacterial growth was examined and recorded the following day.

2.4.3 Minimum Bactericidal Concentration

The Minimum Bactericidal Concentration (MBC) was determined by plating samples from the MIC assay that had concentrations above the MIC value. A 10 µL aliquot from each suspension was inoculated onto MHA and incubated under the same conditions: overnight at 37°C for *E. coli* and *S. aureus*, and for 4 to 7 days under anaerobic conditions for *C. acnes*. The MBC was defined as the lowest concentration of the sample that resulted in complete inhibition of bacterial growth. In cases where partial inhibition was observed, the samples were serially diluted to determine the endpoint concentration required to achieve bactericidal activity.

3.0 RESULTS AND DISCUSSION

3.1 Biosynthesis of Silver Nanoparticles Incorporated Kaolinite

The synthesis of AgNPs using *P. odorata* extract was optimized by evaluating two key parameters: the volume of plant extract and the reaction temperature. The synthesis conditions were fixed with a silver nitrate concentration of 1 mM in a 10 mL solution, and the *P. odorata* extract was used at a concentration of 2% (w/v). The formation of AgNPs was monitored using UV-Visible spectroscopy, which enabled the detection of surface plasmon resonance (SPR), a characteristic phenomenon of metal nanoparticles, resulting from the collective oscillation of conduction electrons in response to incident light (Elemike et al., 2016). The UV-Vis spectra confirmed AgNP formation with a distinct SPR absorption peak centered around 431 nm. Figure 1(a) shows the SPR response for different volumes of *P. odorata* extract, while Figure 1(b) illustrates the SPR shifts observed under varying reaction temperatures. A visible color change from translucent to dark brown further indicated the successful reduction of Ag^+ ions to AgNPs, as illustrated in Figure 2.

As shown in Figure 1(a), the use of 0.6 mL of *P. odorata* extract at 27°C produced the highest SPR intensity at 431 nm, indicating this volume as optimal for AgNP formation. Therefore, 0.6 mL was selected for further analysis involving different reaction temperatures. Figure 1(b) presents the SPR spectra recorded at various temperatures, with the highest intensity observed at 80°C. The increase in SPR intensity at this temperature is attributed to enhanced reaction kinetics

facilitated by thermal energy, which accelerates the reduction of Ag^+ ions and promotes nanoparticle nucleation. The SPR peak at 80°C was sharp and narrow, suggesting that the biosynthesized AgNPs were relatively uniform in size and well-dispersed (Elemike et al., 2016). In contrast, the SPR intensity at 50°C was lower than at 27°C, possibly due to inadequate thermal input to drive efficient reduction. Moreover, red-shifted SPR peaks were observed at 50°C and 27°C, indicating particle agglomeration and increased size distribution. This observation is consistent with the findings of Agustina et al. (2021), who reported a similar red shift due to AgNP clustering. Based on these results, the optimal conditions for the green synthesis of AgNPs using *P. odorata* extract were determined to be 0.6 mL of extract at a reaction temperature of 8 °C.

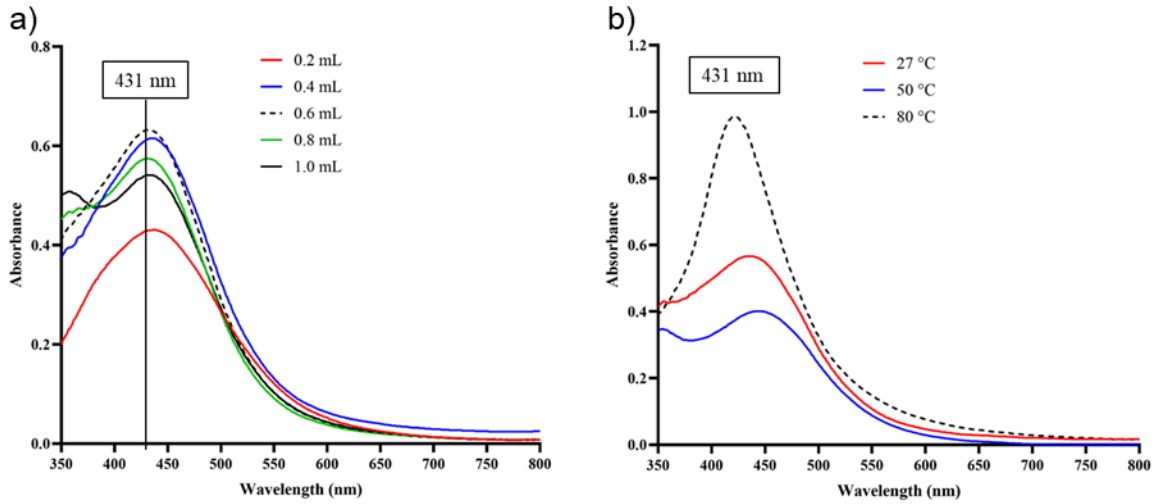

Figure 1 UV-Visible spectra showing (a) the effect of different volumes of *P. odorata* extract on AgNP formation and (b) the influence of reaction temperature on SPR intensity during AgNPs synthesis.

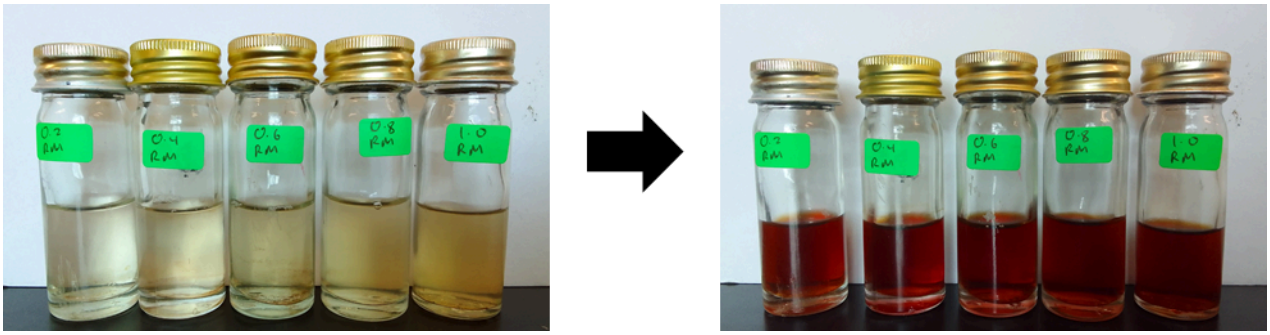

Figure 2 Visual observation of color change before and after the addition of *P. odorata* extract to silver nitrate solution, indicating the formation of AgNPs.

3.2 Samples Characterization

3.2.1 Fourier-Transform Infrared spectroscopy

The synthesized samples (K-AgNP-Kaol, Kesum-Kaol, and Ag-Kaol) were characterized using FTIR spectroscopy to identify the functional groups present in the composites. Figure 3 presents the FTIR spectra of the samples in a stacked format for comparison. The spectral profiles revealed similar absorption patterns between 400 and 1300 cm^{-1}, corresponding to the fingerprint region of kaolinite. A prominent peak observed around 1000 cm^{-1} is assigned to the stretching vibrations of Si–O–Si and Si–O–Al bonds, indicating the structural stability of the aluminosilicate framework of kaolinite. All three samples also exhibited broad absorption bands between 3500 and 3700 cm^{-1}, attributed to O–H stretching vibrations, and weak peaks near 2000 and 1619 cm^{-1}, which are associated with C–H bending vibrations of aromatic compounds derived from the plant extract (Asraf et al., 2024).

Importantly, the FTIR spectra of the modified samples did not show significant changes in the characteristic bands of kaolinite, suggesting that the incorporation of AgNPs and *P. odorata* extract did not alter the fundamental structure of the kaolinite. Since FTIR detects molecular vibrations that involve dipole moments, the metallic bonding characteristic of AgNPs is not observable in the spectra. As a result, the direct detection of AgNPs in K-AgNP-Kaol by FTIR was not possible. Therefore, additional characterization techniques were employed to confirm the successful incorporation of AgNPs into the kaolinite matrix.

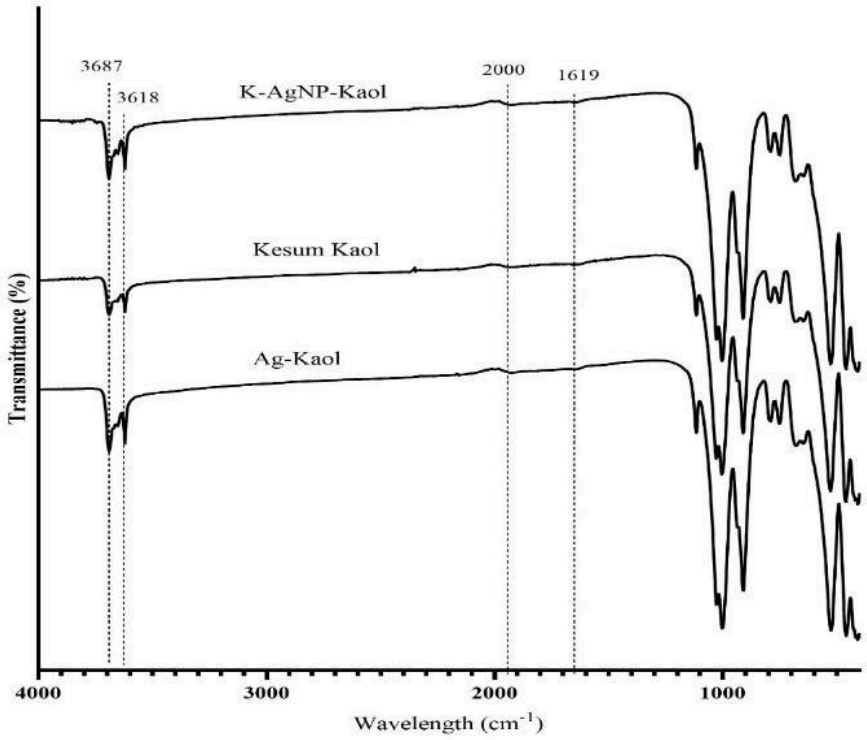

Figure 3 FTIR spectra for K-AgNp-Kaol, Kesum Kaol, and Ag-Kaol

3.2.2 Field Emission Scanning Electron Microscopy and Transmission Electron Microscopy analysis

Figure 4 presents the FESEM images of Ag-Kaol and K-AgNP-Kaol. Both samples display the characteristic plate-like, multilayered morphology typical of kaolinite, consistent with previous reports (Isah et al., 2025). The addition of AgNPs appears to occur via intercalation between the kaolinite layers. Notably, no significant morphological changes were observed in the kaolinite structure after modification, indicating the structural integrity of the clay was preserved, as supported by FTIR analysis. In the Ag-Kaol sample, silver particles were not visibly detected, likely due to the ion-exchange interaction between Ag^+ ions and oxygen atoms within the kaolinite framework, which results in silver being embedded within the layers (Asraf et al., 2024). In contrast, the FESEM image of K-AgNP-Kaol reveals distinct spherical clusters situated between the kaolinite layers, which are attributed to the formation of AgNPs. This provides visual confirmation of successful AgNP incorporation into the kaolinite matrix.

TEM analysis, shown in Figure 5, further confirms the distribution of AgNPs within the K-AgNP-Kaol sample. The nanoparticles were observed on the kaolinite surface, supporting the FESEM findings. The AgNPs exhibited a predominantly spherical shape with diameters ranging from approximately 10 to 60 nm. According to Isah et al. (2025), the adsorption of silver onto kaolinite is facilitated by the net negative charge present on the mineral's basal surfaces and fractured edges. The kaolinite structure consists of multilayered sheets comprising tetrahedral silicon–oxygen (Si–O) and octahedral aluminum–hydroxyl (Al–OH) units, held together by hydrogen bonding (Wang et al., 2024). The Si–O–Si linkages contribute to a negative surface charge, while exposed Al–OH groups at broken edges further enhance this charge, promoting electrostatic attraction and binding of silver species. These results collectively indicate that AgNPs were successfully deposited without compromising the structural framework of kaolinite.

3.2.3 Energy Dispersive X-Ray Analysis

EDX analysis was performed on the surface of the modified kaolinite samples to confirm the elemental composition and ensure the successful incorporation of AgNPs. Measurements were taken at randomly selected points to provide a representative overview of the material. The EDX spectrum of the K-AgNP-Kaol sample, shown in Figure 6, displays the characteristic elemental peaks of kaolinite, including oxygen (O), aluminum (Al), and silicon (Si). Importantly, a distinct peak corresponding to silver (Ag) was also detected, confirming the presence of AgNPs within the kaolinite matrix. Additionally, carbon (C) was identified in the spectrum, which is attributed to organic compounds and functional groups originating from the

P. odorata extract used in the biosynthesis process (Isah et al., 2025). Quantitative analysis revealed a silver content of approximately 0.9 wt%, further validating the successful integration of AgNPs into the kaolinite structure.

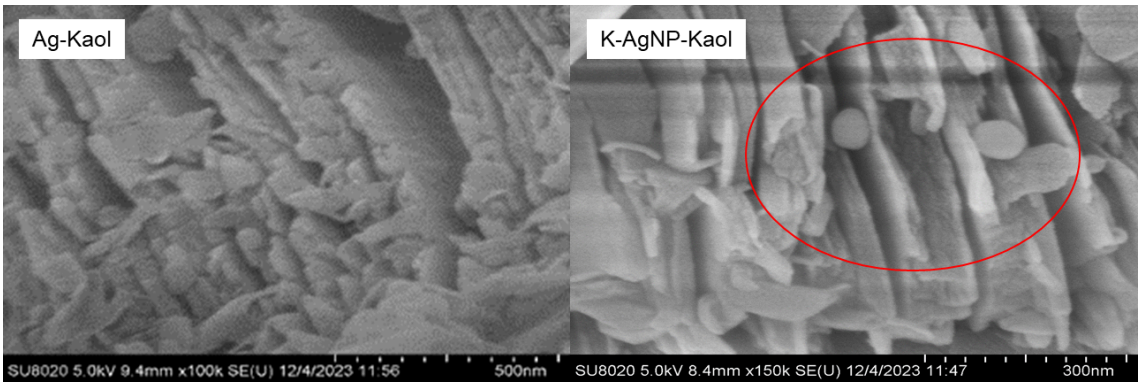

Figure 4 FESEM images of Ag-Kaol and K-AgNP-Kaol.

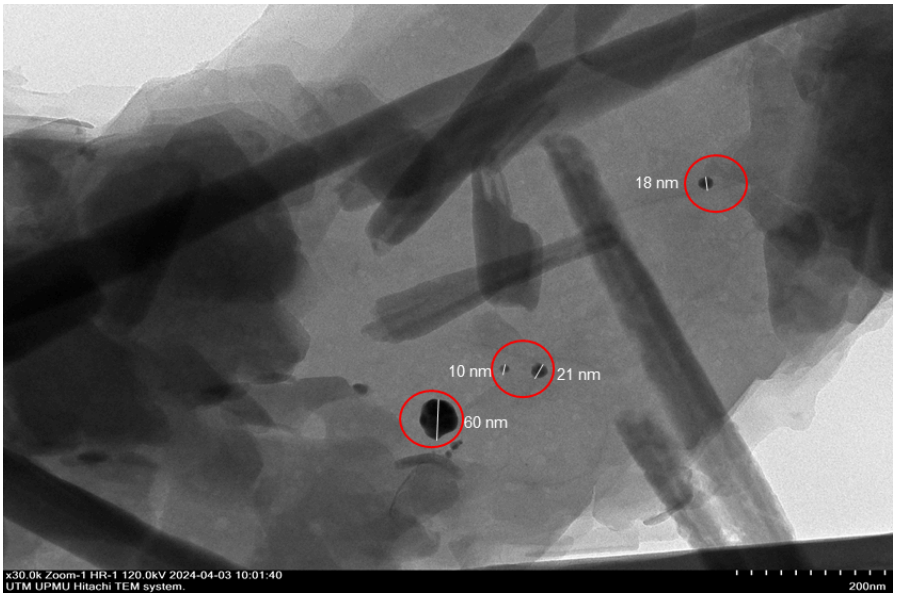

Figure 5 TEM image of K-AgNP-Kaol

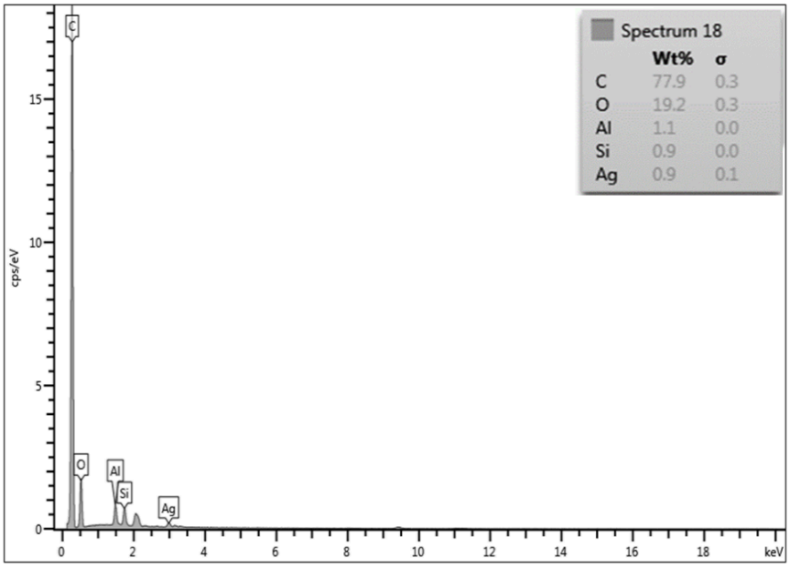

Figure 6 EDX spectrum of K-AgNP-Kaol

3.3 Antimicrobial Activity

3.3.1 Disc Diffusion Technique

Figure 7 presents the top-down view of the inhibition zones obtained from the disc diffusion test (DDT) conducted to evaluate the antibacterial activity of various samples. In addition, 2% *P. odorata* leaf extract (PE) and standard antibiotics, which are Cefoxitin (CF) and Ampicillin (AMP), were included as reference controls.

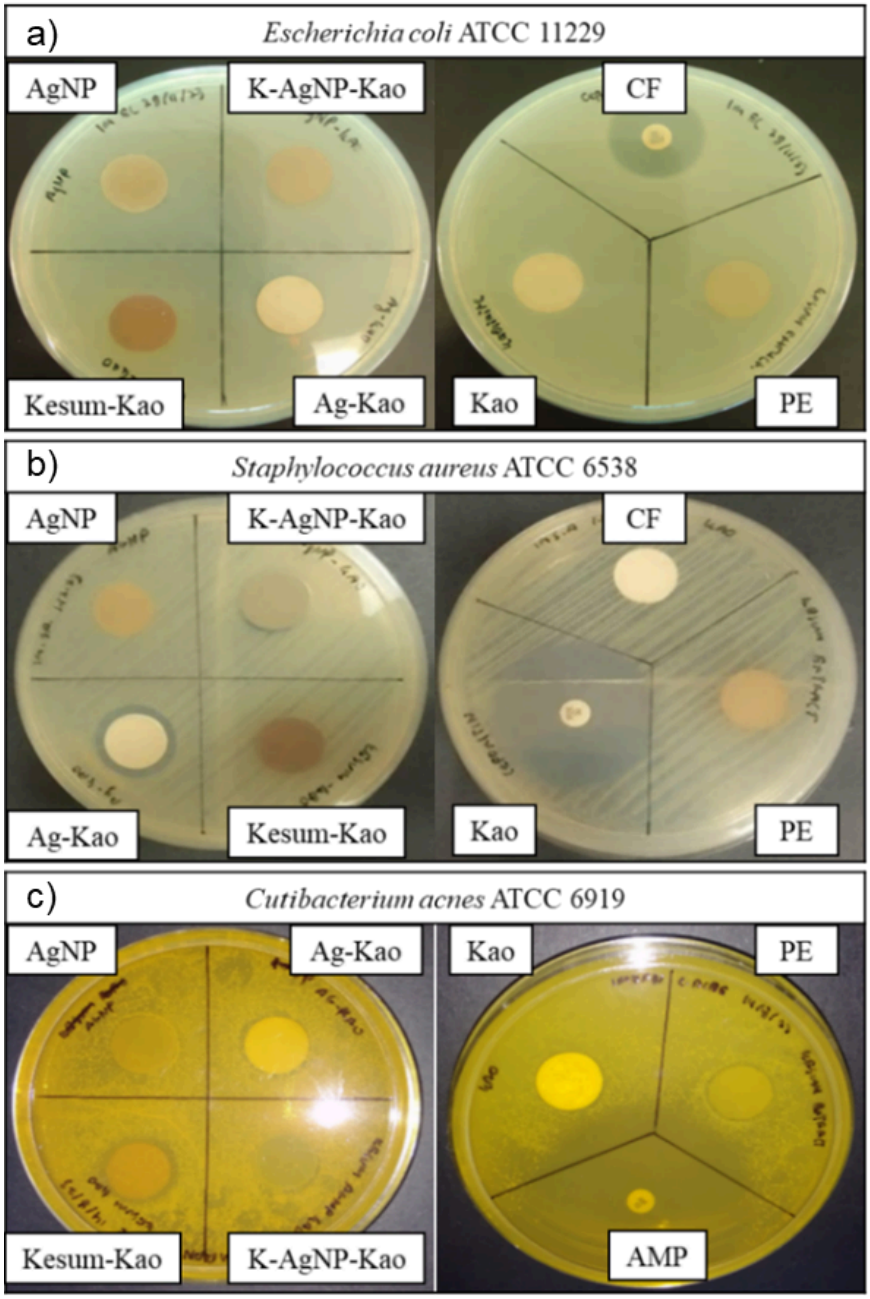

Figure 7 Images of the DDT

As shown in Figure 7(a), no inhibition zones were observed for *E. coli* with any of the tested samples, including kaolinite (Kaol), Kesum-Kaol, Ag-Kaol, and K-AgNP-Kaol. In contrast, the positive control Cefoxitin (CF) exhibited a clear inhibition zone, confirming its effectiveness and validating the assay. The lack of observable antibacterial activity in the test samples suggests that *E. coli* exhibits a high level of resistance to both the silver-based and plant-derived treatments under the tested conditions.

In the case of *S. aureus*, both Ag-Kaol and K-AgNP-Kaol demonstrated inhibitory effects, with Ag-Kaol producing a more pronounced inhibition zone than K-AgNP-Kaol. Other samples, including Kaol, Kesum-Kaol, colloidal AgNP, and *P.*

odorata extract, did not show measurable zones of inhibition, indicating minimal or no activity against *S. aureus*.

For *C. acnes*, inhibition zones were observed for several samples, including Kesum-Kaol, Ag-Kaol, K-AgNP-Kaol, and *P. odorata* extract. Among these, Kesum-Kaol exhibited the most distinct inhibition zone, highlighting the potential antibacterial efficacy of the plant extract against *C. acnes*. The presence of inhibition zones for both Ag-Kaol and K-AgNP-Kaol further supports the antimicrobial contribution of silver. However, the zone formed by K-AgNP-Kaol was notably less prominent, suggesting a weaker antibacterial effect compared to Ag-Kaol. This difference may be attributed to the slower release profile of AgNPs compared to ionic silver.

The control samples, namely kaolinite and *P. odorata* extract, did not exhibit antibacterial activity against *E. coli* or *S. aureus*, but showed limited efficacy against *C. acnes*. As shown in Figure 7, *C. acnes* displayed susceptibility to the *P. odorata* extract, with a measurable inhibition zone of approximately 0.3 cm. Similarly, the Kesum-Kaol sample demonstrated antibacterial activity against *C. acnes*, which is likely attributed to the presence of phytochemical compounds in the plant extract. This observation is supported by previous findings that reported the antimicrobial properties of *P. odorata* (Ridzuan et al., 2013).

Among all tested samples, Ag-Kaol exhibited the most prominent antibacterial activity, producing inhibition zones of 0.5 cm and 0.2 cm against *S. aureus* and *C. acnes*, respectively. This high activity is primarily due to the rapid release of Ag^+ ions from the Ag-Kaol composite, which facilitates immediate interaction with bacterial membranes. In comparison, K-AgNP-Kaol also displayed antibacterial effects against the same bacterial strains, although with smaller inhibition zones. This reduced efficacy is likely due to the slower, sustained release of silver from AgNPs embedded in the kaolinite matrix, resulting in a less immediate antimicrobial response (Asraf et al., 2024). No inhibition zones were observed for *E. coli* in any of the silver or plant-treated samples, indicating a high level of resistance in this Gram-negative strain, with only the positive control (Cefoxitin) showing a significant inhibitory effect.

The antibacterial mechanism of the AgNP-based composites is attributed to the oxidative dissolution of AgNPs, releasing Ag^+ ions that play a central role in disrupting bacterial cell functions. These ions interact with the negatively charged bacterial membrane through electrostatic attraction and ligand-binding interactions (Dutta & Wang, 2019). In addition, the nanoscale size of AgNPs enables them to penetrate bacterial membranes and interfere with channel proteins, leading to cell wall disruption, membrane rupture, and impairment of cellular respiration (Vila Domínguez et al., 2020). AgNPs are also known to generate reactive oxygen species (ROS), further inducing oxidative stress and cytotoxicity within bacterial cells (Wang et al., 2023). Overall, the combined action of Ag^+ ions and AgNPs effectively compromises bacterial membrane integrity and biofilm formation, ultimately leading to cell death.

3.3.2 Minimum Inhibition Concentration

The antimicrobial activity of all tested samples was assessed by determining their MIC against both Gram-negative and Gram-positive bacteria in 0.9% saline solution and distilled water, as shown in Table 1. The results indicate that the presence of electrolytes, particularly in saline solution, reduced the effectiveness of the antimicrobial agents. This suggests that the ionic environment plays a significant role in modulating the antibacterial activity of the silver-containing samples.

Table 1 MIC/MBC againts Gram negative and Gram positive bacteria

	Sample	Concentration (g/L)																
		dH_2O									0.9% saline solution							
		0.2	0.4	0.6	0.8	1.0	3.0	6.0	9.0	12.0	0.2	0.4	0.6	0.8	1.0	3.0	6.0	9.0	12.0
E. coli ATCC 11229	Kaol	■	■	■	■	/	/	/	/	/	■	■	■	■	/	/	/	/	/
	Ag-Kaol	/	*	*	*	*	*	*	*	*	/	/	/	/	/	/	/	/	/
	Kesum Kaol	■	■	■	■	/	/	/	/	/	■	■	■	■	/	/	/	/	/
	K-AgNP-Kaol					/	/	/	*	*					/	/	/	/	/
	Sample	Concentration (g/L)																
		dH_2O									0.9% saline solution							
		0.2	0.4	0.6	0.8	1.0	3.0	6.0	9.0	12.0	0.2	0.4	0.6	0.8	1.0	3.0	6.0	9.0	12.0
S. aureus ATCC 6538	Kaol	■	■	■	■	/	/	/	/	/	■	■	■	■	/	/	/	/	/
	Ag-Kaol	/	/	/	/	*	*	*	*	*	/	/	/	/	/	/	/	/	/
	Kesum Kaol	■	■	■	■	/	/	/	/	/	■	■	■	■	/	/	/	/	/
	K-AgNP-Kaol					/	/	/	*	*					/	/	/	/	/
	Sample	Concentration (g/L)																
		dH_2O									0.9% saline solution							
		0.2	0.4	0.6	0.8	1.0	3.0	6.0	9.0	12.0	0.2	0.4	0.6	0.8	1.0	3.0	6.0	9.0	12.0
C. acnes ATCC 6919	Kaol	■	■	■	■	/	/	/	/	/	■	■	■	■	/	/	/	/	/
	Ag-Kaol	/	/	/	/	/	/	/	/	*	/	/	/	/	/	/	/	/	/
	Kesum Kaol	■	■	■	■	/	/	/	/	/	■	■	■	■	/	/	/	/	/
	K-AgNP-Kaol					/	/	/	*	*					/	/	*	*	*

Notes: (*) Absolute inhibition (/) presence of colonies (blank section) Blank cells (shaded in black and grey) indicate that no test was conducted for the corresponding concentration. This was due to the absence of any antibacterial activity at higher concentrations, suggesting that further testing at lower concentrations would be redundant.

Table 1 shows that neither Kaolinite nor Kesum-Kaol exhibited any inhibitory effect against the tested bacterial strains

across all concentrations. In contrast, Ag-Kaol demonstrated notable antibacterial activity. For *E. coli*, inhibition was observed at a relatively low concentration of 0.4 g/L in distilled water, whereas no inhibition occurred in 0.9% saline solution. Similarly, for *S. aureus* and *C. acnes*, bacterial growth was inhibited in distilled water at concentrations of 1.0 g/L and 12 g/L, respectively, but no inhibitory effect was detected in saline. The absence of activity in saline is attributed to the interaction between Ag^+ ions and Cl^- ions, which results in the formation of silver chloride (AgCl), an insoluble compound that passivates Ag^+ ions and reduces their antimicrobial availability (Stanković et al., 2024).

MIC and MBC analysis for *S. aureus* further confirmed the efficacy of Ag-Kaol, with both values recorded at the lowest tested concentration of 1 g/L. In distilled water, K-AgNP-Kaol also demonstrated antibacterial activity, albeit at a higher concentration of 9 g/L. No inhibition was observed for this sample in saline. Interestingly, *C. acnes* displayed some susceptibility to K-AgNP-Kaol in saline, with MIC and MBC values starting at 6 g/L and 9 g/L, respectively. These findings emphasize the significant impact of the surrounding medium on the antimicrobial performance of silver-based materials. In saline, the presence of chloride ions promotes AgCl formation, which diminishes the release and bioavailability of Ag^+ and AgNPs. In contrast, distilled water, lacking such competing ions, allows silver species to remain bioavailable, thereby enhancing antimicrobial efficacy, a trend consistent with previous findings by Isah et al. (2025).

4.0 CONCLUSION

This study demonstrated the successful green synthesis of silver nanoparticle-incorporated kaolinite (K-AgNP-Kaol) using *P. odorata* leaf extract as a natural reducing agent. Characterization confirmed effective AgNP integration without disrupting the kaolinite structure. Antibacterial testing showed selective activity against *S. aureus* and *C. acnes*, while *E. coli* remained resistant. MIC and MBC results highlighted the enhanced efficacy in distilled water due to reduced Ag^+ ion passivation. Overall, K-AgNP-Kaol shows promise as a sustainable antibacterial material, particularly for Gram-positive bacteria. Further studies are recommended to optimize nanoparticle loading, assess long-term stability, and evaluate biocompatibility for biomedical and environmental use.

Acknowledgment

The authors would like to acknowledge the financial support from the Ministry of Education Malaysia, Universiti Teknologi Malaysia, and Universitas Negeri Malang, Indonesia under the Matching Grant QJ13000.3009.04M28.

References

Agustina, T. E., Handayani, W., & Imawan, C. (2021). The UV-VIS spectrum analysis from silver nanoparticles synthesized using *Diospyros maritima* Blume. leaves extract. *Advances in Biological Sciences Research, 18*, 411–419. https://doi.org/10.2991/absr.k.210621.070

Asraf, M. H., Malek, N. A. N. N., Radzi, M. R. M., & Susanto, H. (2024). Biosynthesized *Persicaria odorata*–silver nanoparticles supported zeolite Y as biocompatible antibacterial agent against *Cutibacterium acnes*. *Particuology, 93*, 1–10. https://doi.org/10.1016/j.partic.2024.05.015

Asraf, M. H., Sani, N. S., Williams, C. D., Jemon, K., & Malek, N. A. N. N. (2022). *In situ* biosynthesized silver nanoparticle-incorporated synthesized zeolite A using *Orthosiphon aristatus* extract for *in vitro* antibacterial wound healing. *Particuology, 67*, 27–34. https://doi.org/10.1016/j.partic.2021.09.007

Chi, M. (1999). Cation exchange capacity of kaolinite. *Clays and Clay Minerals, 47*(2), 174–180. https://doi.org/10.1346/CCMN.1999.0470207

Dakal, T. C., Kumar, A., Majumdar, R. S., & Yadav, V. (2016). Mechanistic basis of antimicrobial actions of silver nanoparticles. *Frontiers in Microbiology, 7*, 1831. https://doi.org/10.3389/fmicb.2016.01831

Din, S. M., Malek, N. A. N. N., Shamsuddin, M., Matmin, J., Hadi, A. A., & Asraf, M. H. (2022). Antibacterial silver nanoparticles using different organs of *Ficus deltoidea* Jack var. *Kunstleri* (King) Corner. *Biocatalysis and Agricultural Biotechnology, 44*, 102473. https://doi.org/10.1016/j.bcab.2022.102473

Dutta, P., & Wang, B. (2019). Zeolite-supported silver as antimicrobial agents. *Coordination Chemistry Reviews, 383*, 1–29. https://doi.org/10.1016/j.ccr.2018.12.014

Elemike, E. E., Onwudiwe, D. C., & Mkhize, Z. (2016). Eco-friendly synthesis of AgNPs using *Verbascum thapsus* extract and its photocatalytic activity. *Materials Letters, 185*, 452–455. https://doi.org/10.1016/j.matlet.2016.09.026

Ijaz, I., Gilani, E., Nazir, A., & Bukhari, A. (2020). Detail review on chemical, physical and green synthesis, classification, characterizations and applications of nanoparticles. *Green Chemistry Letters and Reviews, 13*(3), 223–245. https://doi.org/10.1080/17518253.2020.1802517

Isah, M., Asraf, M. H., Malek, N. A. N. N., Jemon, K., Sani, N. S., Muhammad, M. S., Wahab, M. F. A., & Saidin, M. A. R. (2020). Preparation and characterization of chlorhexidine modified zinc-kaolinite and its antibacterial activity against bacteria isolated from water vending machine. *Journal of Environmental Chemical Engineering, 8*(2), 103545. https://doi.org/10.1016/j.jece.2019.103545

Isah, M., Malek, N. A. N. N., Susanto, H., Asraf, M. H., & Aliero, A. S. (2025). Preparation, characterization, and antibacterial activity of *Moringa oleifera*–silver nanoparticles–kaolinite nanocomposite. *Applied Clay Science, 269*, 107761.

https://doi.org/10.1016/j.clay.2025.107761

Li, X., Xu, H., Chen, Z.-S., & Chen, G. (2011). Biosynthesis of nanoparticles by microorganisms and their applications. *Journal of Nanomaterials, 2011*, Article ID 270974. https://doi.org/10.1155/2011/270974

Lubis, F. A., Malek, N. A. N. N., Sani, N. S., & Jemon, K. (2022). Biogenic synthesis of silver nanoparticles using *Persicaria odorata* leaf extract: Antibacterial, cytocompatibility, and *in vitro* wound healing evaluation. *Particuology, 70*, 10–19. https://doi.org/10.1016/j.partic.2022.01.001

Ridzuan, P. M., Hairul Aini, H., Norazian A. Shah, M. H., Roesnita, & Aminah, K. S. (2013). Antibacterial and antifungal properties of *Persicaria odorata* leaf against pathogenic bacteria and fungi. *The Open Conference Proceedings Journal, 4*(1), 71–75. https://benthamopen.com/ABSTRACT/TOPROCJ-4-2-71

Stanković, M., Kljun, J., Stevanović, N. L., Lazić, J., Bogojević, S. S., Vojnović, S., Zlatar, M., Nikodinović-Runić, J., Turel, I., Djuran, M. I., & Glišić, B. Đ. (2024). Silver(I) complexes containing antifungal azoles: Significant improvement of the anti-*Candida* potential of the azole drug after its coordination to the silver(I) ion. *Dalton Transactions, 53*(5), 2218–2230. https://doi.org/10.1039/D3DT03010E

Tan, D., Yuan, P., Annabi-Bergaya, F., Dong, F., Liu, D., & He, H. (2015). A comparative study of tubular halloysite and platy kaolinite as carriers for the loading and release of the herbicide amitrole. *Applied Clay Science, 114*, 190–196. https://doi.org/10.1016/j.clay.2015.05.024

Vila Domínguez, A., Ayerbe Algaba, R., Miró Canturri, A., Rodríguez Villodres, Á., & Smani, Y. (2020). Antibacterial activity of colloidal silver against Gram-negative and Gram-positive bacteria. *Antibiotics, 9*(1), 36. https://doi.org/10.3390/antibiotics9010036

Wang, J., Fu, L., & Yang, H. (2024). Structural modulation of kaolinite nanoclay via DFT and molecular dynamics simulations: A review. *Applied Clay Science, 258*, 107473. https://doi.org/10.1016/j.clay.2024.107473

Wang, W., Yu, Z., Lin, M., & Mustapha, A. (2023). Toxicity of silver nanoparticle-incorporated bacterial nanocellulose to human cells and intestinal bacteria. *International Journal of Biological Macromolecules, 241*, 124705. https://doi.org/10.1016/j.ijbiomac.2023.124705